

Visualization of The Initiation and Stabilization Process of an Oblique Detonation Wave Around a Projectile

Shinichi Maeda¹, Jiro Kasahara¹, Akiko Matsuo²

¹Department of Engineering Mechanics and Energy, University of Tsukuba
1-1-1 Tennodai, Tsukuba, 305-8573, Japan

²Department of Mechanical Engineering, Keio University
3-14-1 Hiyoshi, Kohoku-ku, Yokohama, 223-8522, Japan

1 Introduction

An oblique detonation wave (ODW) occurs in a hypersonic detonable mixture flow or around a hypersonic projectile flying in a detonable mixture at rest, when the flow or projectile velocities are higher than propagation velocities of detonation waves. An oblique detonation wave engine (ODWE) [1] or ram-accelerator (RAMAC) [2, 3] in which an ODW is stabilized in a combustor have a continuous combustion process in contrast to a pulse detonation engine (PDE). These engines are expected to achieve short combustors for hypersonic flight engines using detonation waves which have almost constant-volume combustion process. One of important issues for these engines is the critical condition and mechanism to initiate and stabilize an ODW. An experimental visualization of a stabilized ODW around a hypersonic projectile was first reported by Lehr [4]. Lee [5] and Vasiljev [6] proposed a criticality equation to initiate a detonation wave by a projectile using hypersonic blast-wave analogy. Experimental studies to investigate initiating or stabilizing criticality have been conducted by Higgins and Bruckner [7], Kaneshige and Shepherd [8], Kasahara *et al.* [9-11], Verreault and Higgins [12] and Maeda *et al.* [13] carrying out optical observations or pressure recordings. Although the stabilized ODW is steady phenomenon, an existence of unsteady detonation wave propagation was suggested at the vicinity of criticality [8, 10] and the unsteady propagation process was directly observed by detailed continuous frames using a high-speed camera [13]. However the wave structure of ODW stabilized around cone-nosed cylinder was first suggested by Kasahara *et al.* [10], the wave structure of unsteady phenomenon at the vicinity of stabilizing criticality has not been reported.

In this study, we launched a spherical projectile into an acetylene / oxygen mixture highly diluted with krypton which had comparatively high mixture density. This allowed high contrast optical observation to investigate the wave structure of an unsteady phenomenon at the vicinity of criticality. In addition, the detailed time history of unsteady detonation initiation process by a projectile was visualized using an acetylene / oxygen mixture diluted with argon. It was investigated that a diffracted shock and combustion wave around the projectile initiated the stabilized ODW.

2 Experimental Setup and Conditions

Hypersonic spherical projectiles were launched into detonable mixtures at rest, and Schlieren visualizations were conducted using a high-speed camera (HPV-1, 312×260 pixels spatial resolution, Shimadzu). The experimental setup [13] consisted of four devices shown as (1) through (4) in Figure 1. The projectiles launched by the gas gun broke a very thin (12- μm thickness) Mylar diaphragm (diaphragm 1 in Figure 1) and entered the observation chamber filled with a detonable mixture. The optical observation region was circular with a 90-mm diameter, and the center of this region was located 400 mm downstream of the chamber inlet. A set of diode laser and photodiode was placed upstream of the observation region, to detect the passing projectile. The detected signal triggered the high-speed camera through a delay generator. A spherical projectile was chosen to eliminate any influence of the flight attitude. The projectile had a 4.76-mm

diameter and was made of polyethylene. The recording conditions of the high-speed camera were a 1- μs frame speed, a 250-ns exposure time and a maximum of 100 continuous shots in all experiments.

The Projectile velocities were always higher than the C-J velocities of ambient detonable mixtures, and the cell widths were several-fold smaller than the projectile diameters, to achieve stabilized ODWs around the projectiles. Detonable mixtures were stoichiometric acetylene / oxygen mixtures ($2\text{C}_2\text{H}_2 + 5\text{O}_2$) diluted with argon ($2\text{C}_2\text{H}_2 + 5\text{O}_2 + 7\text{Ar}$) or krypton ($2\text{C}_2\text{H}_2 + 5\text{O}_2 + 21\text{Kr}$) in a 50% or 75% volumetric fraction to lower the C-J velocity of the mixture. Experimental conditions expressed by non-dimensional projectile velocities (ratios of the projectile velocity V_p to the C-J velocity D_{CJ} , V_p / D_{CJ}) and non-dimensional projectile diameters (ratios of the projectile diameter and the cell width, d / λ) are listed in Table 1. Critical non-dimensional projectile diameters for stabilizing ODWs were investigated by varying the filling pressures (the cell widths). Filling temperatures of the mixtures were kept room temperatures, $T_0 = 292.5 \pm 5.1$ K. The experimental results of Desbordes and Desbordes *et al.* [14, 15] for the cell sizes were accessed from the Detonation Database (Kaneshige and Shepherd [16]). Fitting equations for these cell sizes (λ [mm]) as an exponential of filling pressures (p_0 [kPa]) gives $\lambda = 61.52 \times p_0^{-1.117}$ for $2\text{C}_2\text{H}_2 + 5\text{O}_2 + 7\text{Ar}$ mixture and $\lambda = 138.4 \times p_0^{-1.206}$ for $2\text{C}_2\text{H}_2 + 5\text{O}_2 + 21\text{Kr}$ mixture, and the cell sizes were interpolated or extrapolated by these equations for each set of experimental conditions. The C-J velocity was calculated using the chemical equilibrium computation software STANJAN (Reynolds

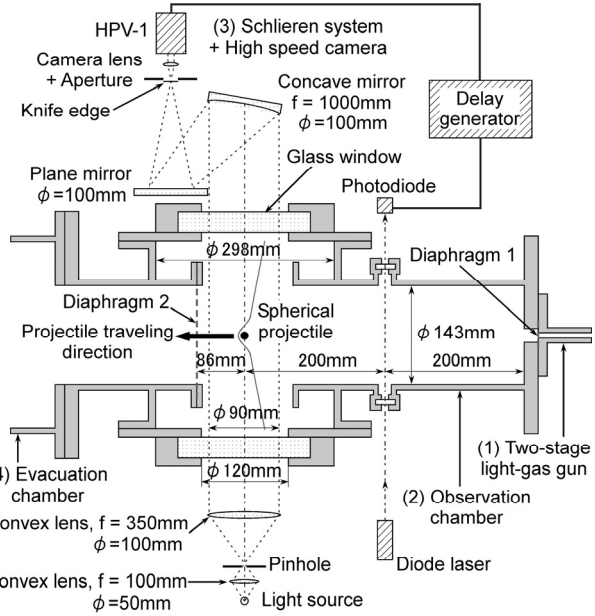


Figure 1. Schematic diagram of the experimental setup (top view).

Table 1. Experimental conditions. Symbols in the “result”: \times : Shock-induced combustion, \triangle : Straw Hat type with attenuated ODW, \circ : Straw Hat type with stabilized ODW, and \bullet : Stabilized ODW.

Mixture	Filling pressure	V_p / D_{CJ}	d / λ	Result	Figure
-	± 0.05 kPa	± 0.65 %	± 0.5 %	-	-
$2\text{C}_2\text{H}_2 + 5\text{O}_2 + 21\text{Kr}$	61.4	1.05	4.93	\times	2 (b)
	70.3	1.11	5.81	\triangle	3 (b)
	72.9	1.10	6.07	\circ	3 (a)
	81.1	1.09	6.90	\bullet	2 (a)
$2\text{C}_2\text{H}_2 + 5\text{O}_2 + 7\text{Ar}$	41.8	1.07	5.01	\bullet	6 and 7

[17]). The Projectile velocities were determined by the time histories of projectile locations using the observed continuous images. The projectile locations were situated almost linearly over time, and thus velocity deficits in the observation region were negligible. The large collection of continuous pictures could show many of the projectile locations with good accuracy, and systematic errors of the projectile velocities were within $\pm 0.65\%$.

3 Wave Structures of Straw Hat types

Figures 2 and 3 show the visualization results in $2\text{C}_2\text{H}_2+5\text{O}_2+21\text{Kr}$ mixture. The non-dimensional projectile velocities were kept at $V_p / D_{\text{CJ}} = 1.08 \pm 0.03$. These are negative pictures, and white circles are the projectiles. The projectile traveling directions are from right to left. Similar trends were observed under the similar non-dimensional projectile velocities using $2\text{C}_2\text{H}_2+5\text{O}_2+7\text{Ar}$ mixture [13].

The ODW was stabilized in Figure 2 (a) and was not initiated, that is shock-induced combustion in Figure 2 (b). The waves were steadily propagating relative to the projectiles. The superposed pictures shown in Figures 3 (a) and (b) show unsteady propagation modes called Straw Hat type [10, 11, 13] observed at the vicinity of criticality for stabilizing ODW. These modes consisted of a shock-induced combustion and C-J ODW. Two types of Straw Hat type were reported by Kasahara *et al.* [10] and Maeda *et al.* [13] whether the C-J ODW was attenuated or stabilized. In these Straw Hat types, the bow-shock was discontinuously connected to the C-J ODW. It was reported that the bow-shock was partially decoupled with the combustion wave in the Straw Hat type whose C-J ODW was attenuated [10], however, the bow-shock was fully coupled with the combustion wave in the Straw Hat type whose C-J ODW was stabilized [13]. In Figure 3 (a), unsteady local explosions near the triple point stabilized the edge of ODW, and the relative distance between the projectile and the ODW edge was fluctuating. However, this unsteadiness near the triple point couldn't be found in Figure 3 (b). Lacking of the mechanism for stabilizing ODW disappear the edge of ODW, and relative distance between the projectile and the ODW edge increase over time. We also measured the wave angles and propagation velocities using the continuous pictures. The wave angles, θ_w , can be related to the propagation velocities, D_w , and projectile velocities, V_p , by the relation $\theta_w = \sin^{-1}(D_w / V_p)$, when the wave propagations are supported by the projectiles and remaining steady. In Figures 2 (a) and 3 (a), the measured wave angles of C-J ODW agreed with its calculated C-J angles. Therefore, the C-J ODWs were supported by the projectiles. However, the measured wave angle of C-J ODW was about 5 % larger than its calculated C-J angle in Figure 3 (b), despite the measured propagation velocity agreed with the C-J velocity calculated by STANJAN. This means the C-J ODW was not supported by the projectile, and the horizontal component of its propagation velocity was lower than the projectile velocity. We call Figure 3 (a) as «Straw Hat type with stabilized ODW», and Figure 3 (b) as «Straw Hat type with attenuated ODW». Only about 2.5 kPa difference of the filling pressures divided these two Straw Hat types. Kasahara *et al.* [10] have visualized the detonation initiation in the «Straw Hat type with attenuated ODW» was affected by the diaphragm rapture at the chamber inlet. We conclude the «Straw Hat type with attenuated ODW» is the transient process, because the C-J ODW was not supported by the projectile, and it will ultimately disappear.

The connection point between the bow-shock and C-J ODW should be tirple point because of their discontinuous connection. Therefore, there should be shock structure inside these Straw Hat types. In

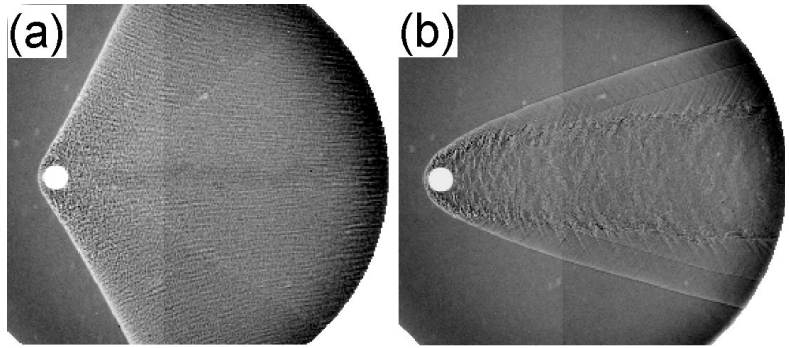


Figure 2. Snapshots of the movies when (a) the ODW was stabilized or (b) was not initiated (shock-induced combustion).
(a): $d / \lambda = 6.90$ and (b): $d / \lambda = 4.93$.

this study, the wave structures are suggested as Figure 4 for Straw Hat type with stabilized ODW and as Figure 5 for Straw Hat type with attenuated ODW. These figures show a central cross section of axisymmetric phenomenon. In both Straw Hat types with attenuated or stabilized ODW, the connection points between the bow-shock and conical C-J ODW are triple points («Transition point» in the figures) and an incident shock propagates from the transition point to a central axis in the burned gas. The incident shocks make Mach intersection near the central axis. However, the shock compressed unburned mixture exists at the decoupling region between the bow-shock and combustion wave in Straw Hat type with attenuated ODW. Therefore, the transverse detonation or shock wave propagates from the transition point to the incident shock. In Figures 3 (a) and (b), the wave structures existing between the transition points and central axes as shown in Figures 4 and 5 are visible.

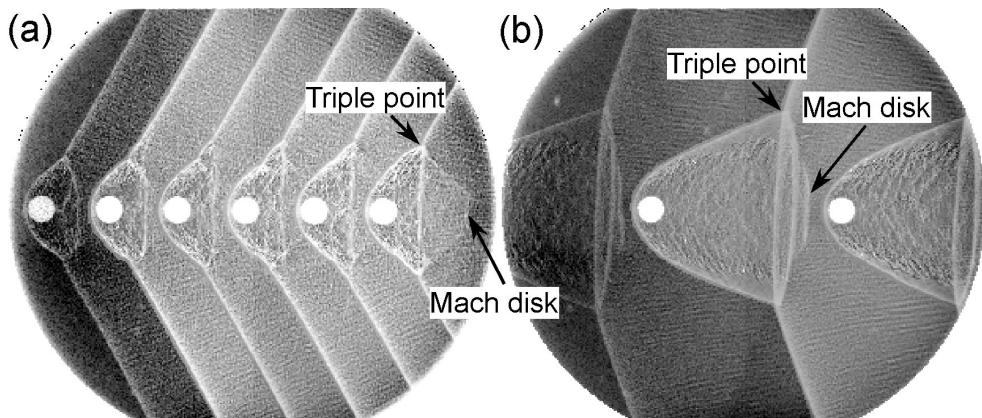


Figure 3. Superposed pictures of the movies of Straw Hat type with
(a) stabilized and (b) attenuated ODW.

(a): $d / \lambda = 6.07$, 9 μs intervals and (b): $d / \lambda = 5.81$, 25 μs intervals.

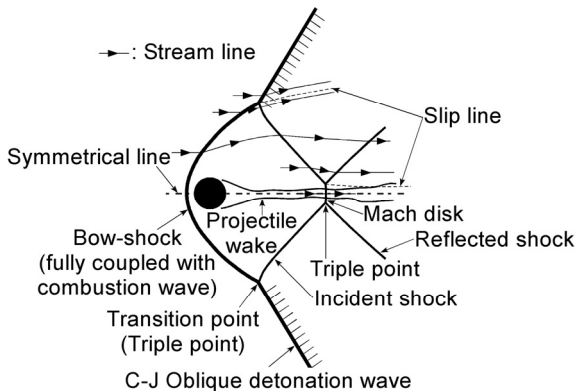


Figure 4. The wave structure of Straw Hat type with stabilized ODW (central cross section of axisymmetric phenomenon).

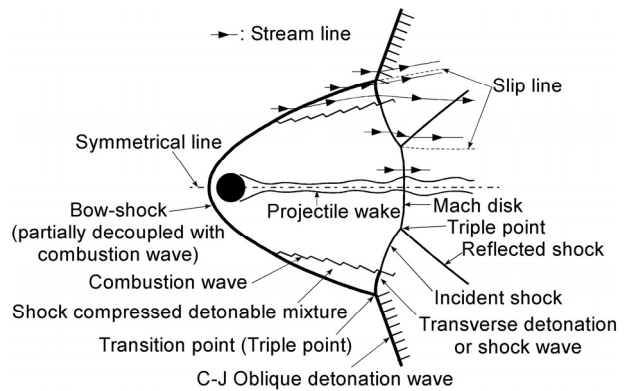


Figure 5. The wave structure of Straw Hat type with attenuated ODW (central cross section of axisymmetric phenomenon).

4 Initiation Process of an Oblique Detonation Wave

Figures 6 and 7 show unsteady initiation processes of the stabilized ODW. In Figure 6, the continuous pictures are shown in time-series and times after the recording start of high-speed camera are shown at upper left in the each picture. In Figure 7, the continuous pictures are superposed with 3 μs intervals. The mixture was $2\text{C}_2\text{H}_2+5\text{O}_2+7\text{Ar}$, and the non-dimensional projectile velocity was almost the same as the results in the former section. A flange was placed in the observation region to set a Mylar diaphragm which had 30-mm diameter and 12- μm thickness as shown in Figure 6. The diaphragm was located at 5-mm upstream of the flange surface. The projectile passed the vacuumed section upstream of this diaphragm and run into the detonable mixture after the diaphragm rapture.

These figures show the detonation initiation process just after the diaphragm rapture. The strong shock wave existed ahead of the projectile, and it was diffracted apart from the projectile. A chemical reaction was initiated by the shock compression, and almost conical C-J ODW was gradually established just around the projectile during 45 μ s to 60 μ s. However, the ODW establishment at far field needed a strong initiation process which was similar to a re-initiation process in a detonation diffraction. You can see this initiation process at 60 μ s. The detonation wave was initiated by the local explosion on the diffracted shock wave. It expanded almost spherically, and its upstream side establishes the ODW front at far field. The curvature radius of detonation wave around the projectile increased as the projectile travelling. And the result of this visualization indicates that the critical curvature radius is needed for stabilizing the ODW at far field. Here, we should notice the effect of diaphragm fragments by the projectile impact. Most of fragments were visible behind the projectile, but the parts of them were flying near the projectile and wave front. The non-dimensional projectile diameter in this result was $d / \lambda = 5.01$, and was well above the critical condition, that is about 3.5 reported by Maeda *et al.* [13]. Therefore, the general initiation process seems to be the same as that without the diaphragm effect. But the diaphragm effect will be much apparent in sensitive conditions near the criticality.

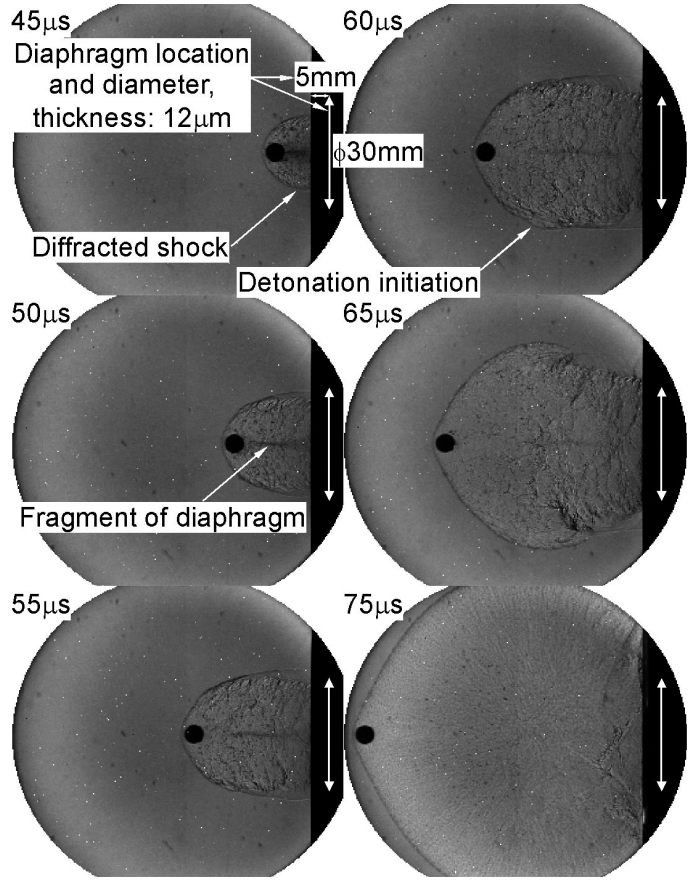


Figure 6. The continuous pictures of unsteady initiation process of the stabilized ODW in $2\text{C}_2\text{H}_2 + 5\text{O}_2 + 7\text{Ar}$ mixture.

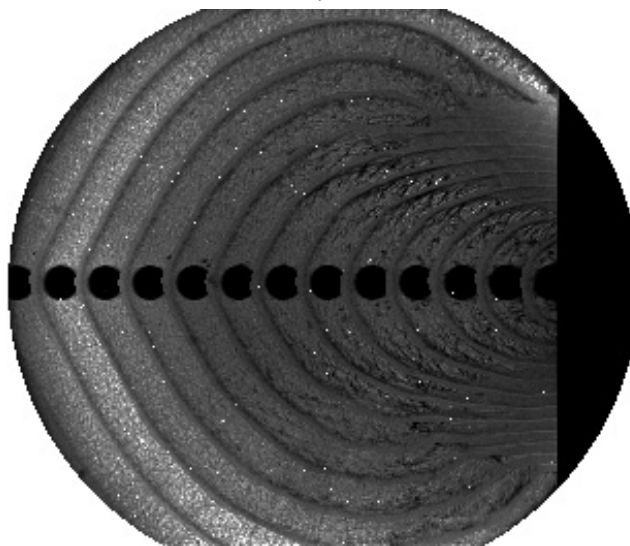


Figure 7. The continuous pictures shown in Figure 6 are superposed at 3 μ s intervals.

5 Conclusions

The stabilization of an ODW around a spherical projectile was visualized. Wave structures of Straw Hat types observed at a vicinity of the stabilization criticality were proposed and confirmed by dozens of continuous pictures. They had triple points at the intersections of a bow-shock and a C-J ODW with a transverse detonation or shock wave. The initiation process just after the diaphragm rapture by the projectile was also visualized. The detonation wave was initiated by the local explosion on the diffracted shock wave. It expanded almost spherically, and its upstream side establishes the ODW front at far field. And the result of this visualization indicates that the critical curvature radius at the initiation point is needed for stabilizing the ODW at far field.

References

- [1] J. M. Powers (1994), Combustion in High-Speed Flows, Kluwer Academic Publishers Boston, 345-371 (ISBN 978-0-7923-2806-3).
- [2] A. Hertzberg, A. P. Bruckner, D. W. Bogdanoff (1988), AIAA J. 26 (2): 195-203.
- [3] A. J. Higgins (2006), J. Propul. Power 22 (6): 1170-1187.
- [4] H.F. Lehr (1972), Astronautica Acta 17: 589-597.
- [5] J. H. S. Lee (1997), Prog. Astronaut. Aeronaut. 173: 293-310.
- [6] A.A. Vasiljev (1994), Shock Waves 3: 321-326.
- [7] A.J. Higgins, and A.P. Bruckner (1996), AIAA paper 96-0342.
- [8] M.J. Kaneshige, J.E. Shepherd (1996), Proc. Combusti. Inst. 26: 3015-3022.
- [9] J. Kasahara, T. Horii, T. Endo, T. Fujiwara (1996), Proc. Combusti. Inst. 26: 2903-2908.
- [10] J. Kasahara, T. Fujiwara, T. Endo, T. Arai (2001), AIAA J. 39 (8): 1553-1561.
- [11] J. Kasahara, T. Arai, S. Chiba, K. Takazawa, Y. Tanahashi, A. Matsuo (2002), Proc. Combusti. Inst. 29: 2817-2824.
- [12] J. Verreault, A.J. Higgins (2011), Proc. Combusti. Inst. 33: 2311-2318.
- [13] S. Maeda, R. Inada, J. Kasahara, A. Matsuo (2011), Proc. Combusti. Inst. 33: 2343-2349.
- [14] D. Desbordes (1988), Prog. Astronaut. Aeronaut. 114: 170-185.
- [15] D. Desbordes, C. Guerraud, L. Hamada, and H.N. Presles (1993), Prog. Astronaut. Aeronaut. 153: 347-359.
- [16] M. J. Kaneshige, J. E. Shepherd (1997), Detonation Database, Technical Report No. FM97-8, GALCIT, Pasadena, CA.
- [17] W. C. Reynolds (1986), The Element Potential Method for Chemical Equilibrium Analysis: Implementation in the Interactive Program STANJAN: Version3, Technical Report No. A-3991, Stanford Univ..